Examining Spatial Variations in California Earthquake Dynamics Using a High- to Low-Frequency Spectral Ratio

Ian Vandevert, Peter Shearer, and Wenyuan Fan

Scripps Institution of Oceanography, UC San Diego (ivandevert@ucsd.edu, pshearer@ucsd.edu, wenyuanfan@ucsd.edu)

Why do earthquakes differ from each other?

Earthquakes of similar magnitude can cause different amounts of shaking. These differences reflect varying earthquake source characteristics, which is **critical for studying hazard**. Stress drop ($\Delta\sigma$) is related to the amount of damaging high-frequency radiation, but their **estimates often have large uncertainties** (see Baltay et al., 2024).

For earthquakes of similar size, **variation in ground motion is due to the relative amount of high-frequency energy compared to low-frequency**. We define a parameter $\log\beta$ to quantify this:

$$\log\beta = \log A_{HF} - \log A_{LF}$$

where A_{HF} is the high-frequency spectral amplitude and A_{LF} is the low-frequency spectral amplitude (**F2**). We correct for station, path, and magnitude effects to obtain the **normalized frequency index**, nFI, which **quantifies an earthquake's high-frequency output relative to the average of nearby M1.5 calibration events.**

We have recently published our results applying this method to P- and S-wave spectra from the 2019 Ridgecrest earthquake sequence (Vandevert et al., 2026, *accepted*). Here, we apply this method to **P-waves from over 750,000 California earthquakes** over a 30-year period and present our preliminary findings.

How does it work?

Step 1: Compute $\log\beta$ for all seismograms

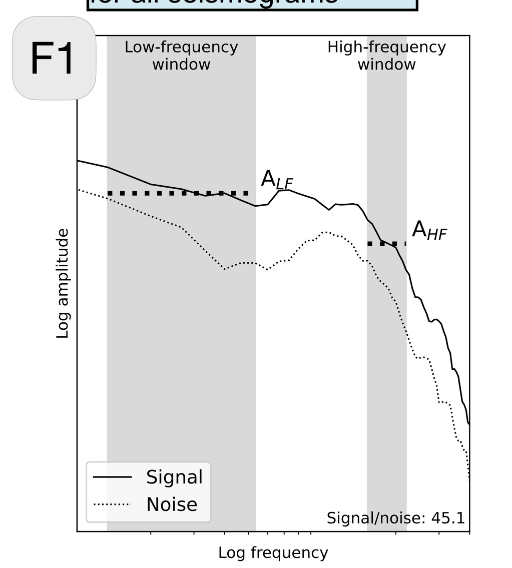

F1: A_{LF} and A_{HF} are computed as the median amplitude of bands 1-5 Hz and 12-20 Hz. Similar to the frequency index (FI, Buurman et al. 2010).

Step 2: Correct for station and path effects to obtain $\Delta\log\beta$, which is measured relative to nearby "calibration" events

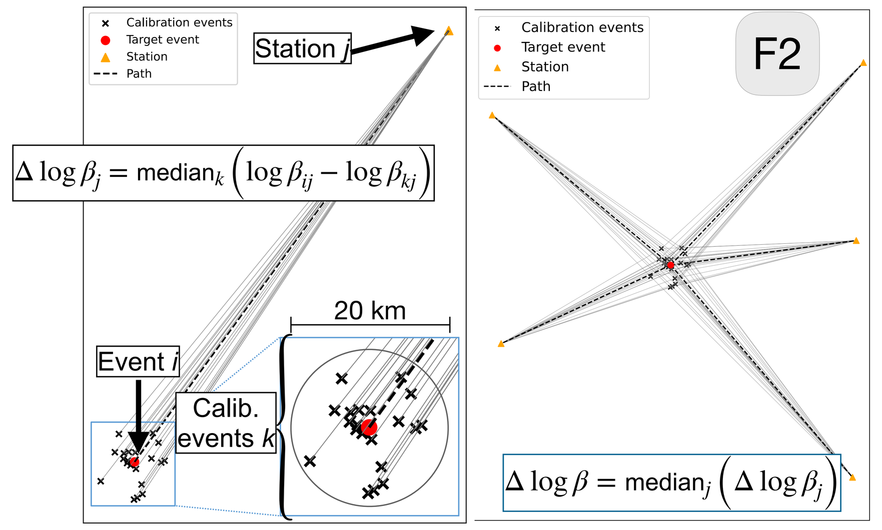

F2: Corrections using nearby M1.4–1.6 calibration events. This is analogous to Shearer et al. (2022), and corrects for station and path effects. Calibration events are within ±2km vertically of target event.

Step 3: Correct for magnitude dependence to get nFI: fit a smoothed empirical correction to $\Delta\log\beta$ vs. magnitude, and subtract from all events

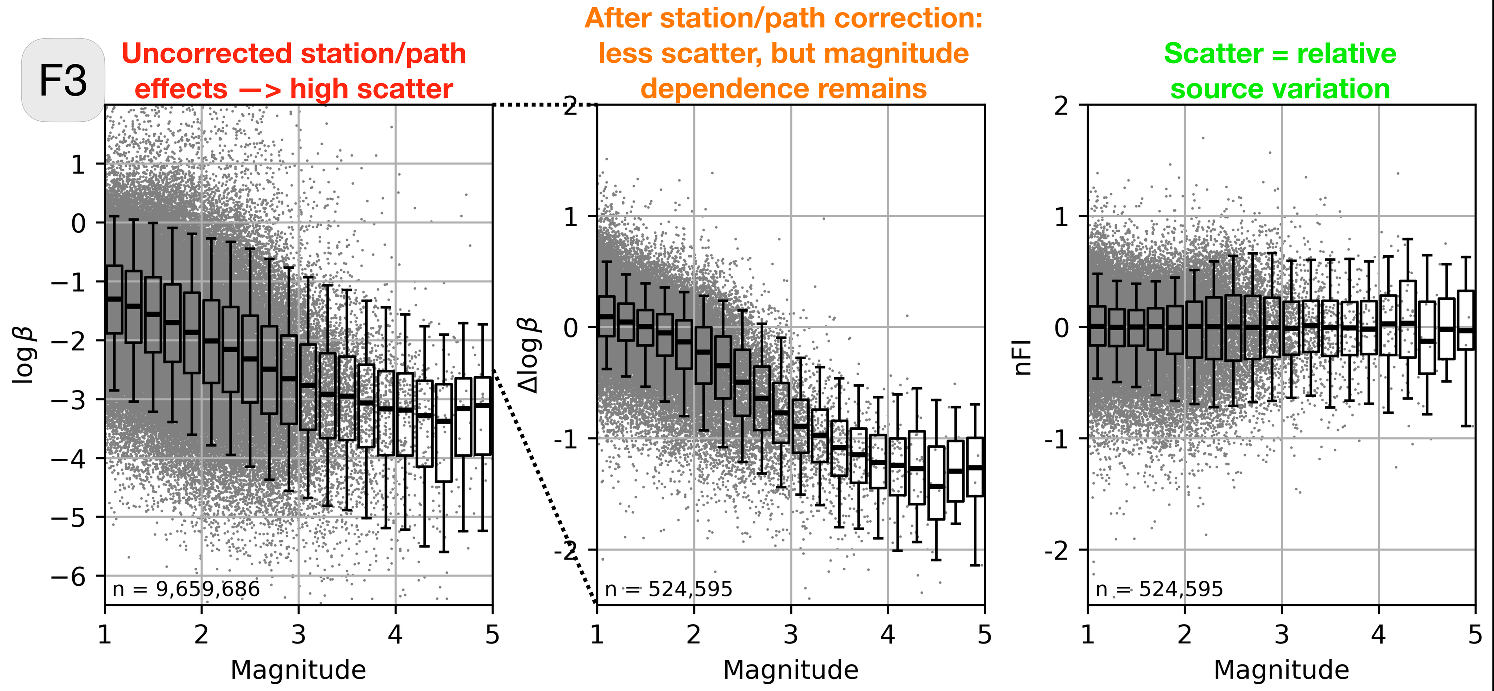

F3: For the entire California dataset, (left) uncorrected $\log\beta$ (similar to FI); (middle) station- and path-corrected $\Delta\log\beta$; and (right) nFI. Magnitude correction is done separately for NCEDC and SCEDC events.

California results display large-scale spatial variation

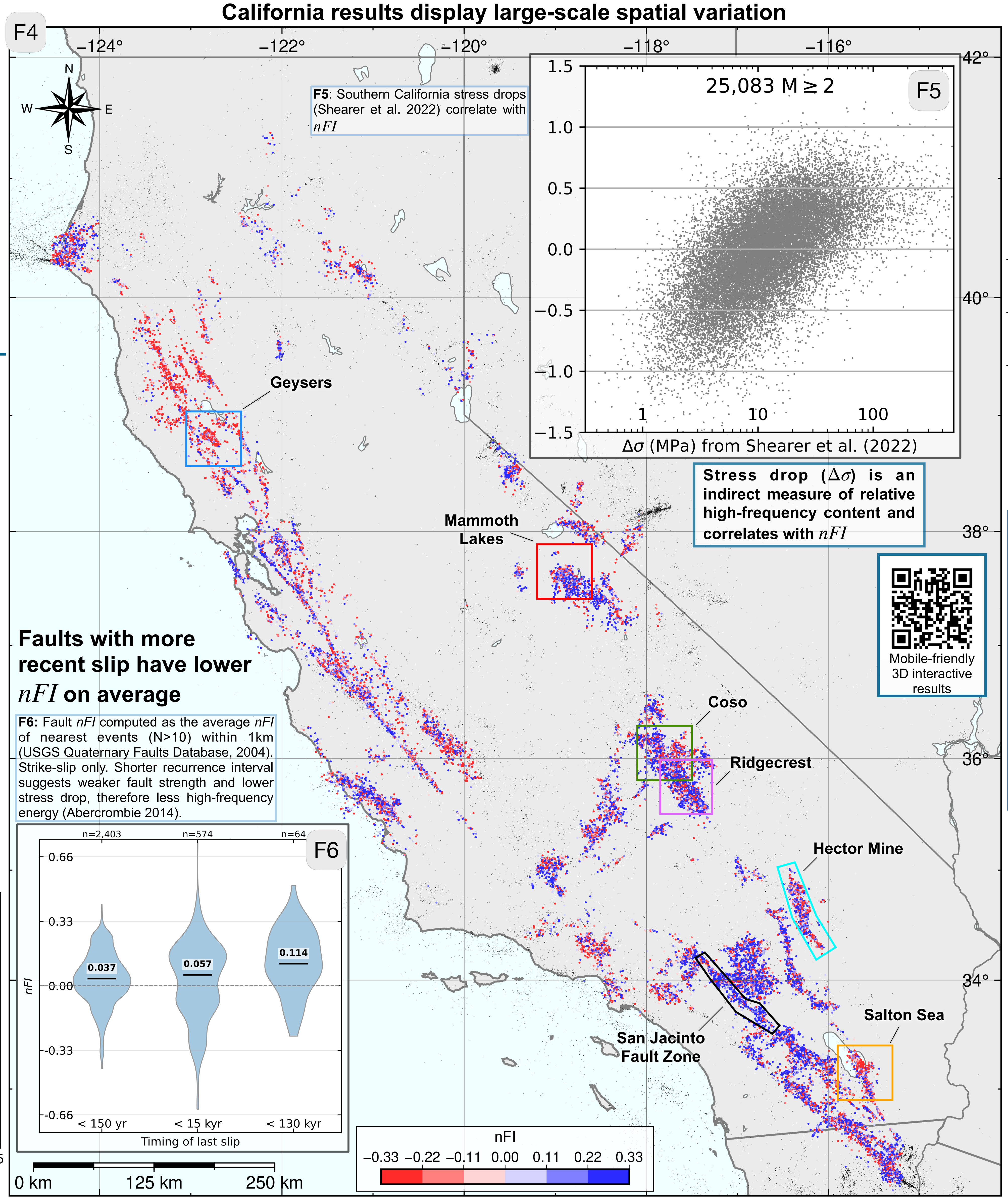

Faults with more recent slip have lower nFI on average

F6: Fault *nFI* computed as the average *nFI* of nearest events (N>10) within 1km (USGS Quaternary Faults Database, 2004). Strike-slip only. Shorter recurrence interval suggests weaker fault strength and lower stress drop, therefore less high-frequency energy (Abercrombie 2014).

F4: Spatial distribution of nFI for earthquakes larger than M2. Earthquakes with nFI estimates shown as color dots (N=97,951). Earthquakes without nFI estimates are shown as black dots (N=63,779). Total earthquakes in catalog larger than M2: 161,738.

nFI correlates with some geophysical parameters

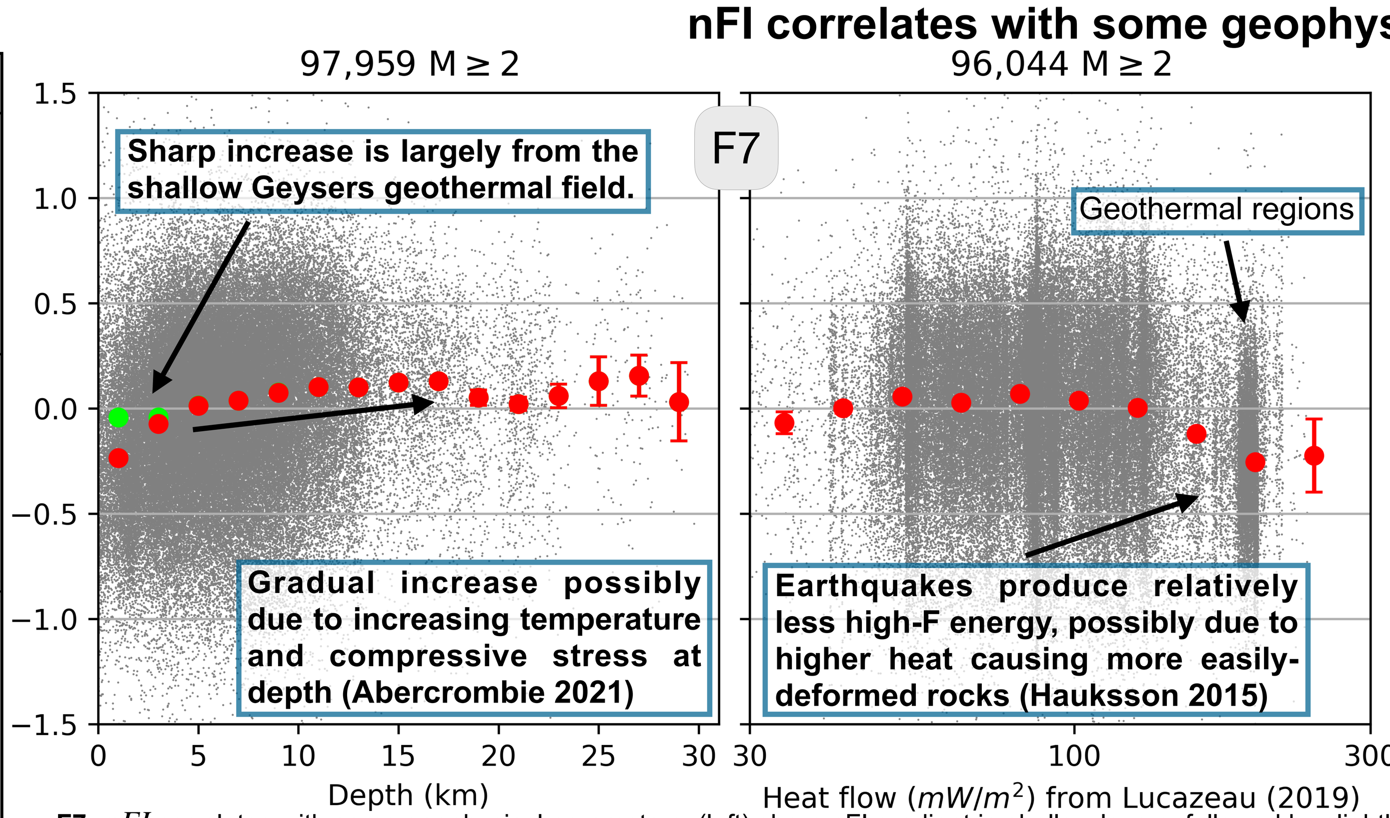

F7: nFI correlates with some geophysical parameters: (left) sharp nFI gradient in shallow layers, followed by slightly increasing nFI with depth. Red markers denote bin median when excluding Geysers geothermal field events; (right) nFI is low in regions with high heat flow. Black markers indicate medians, whiskers indicate $2\times$ standard error.

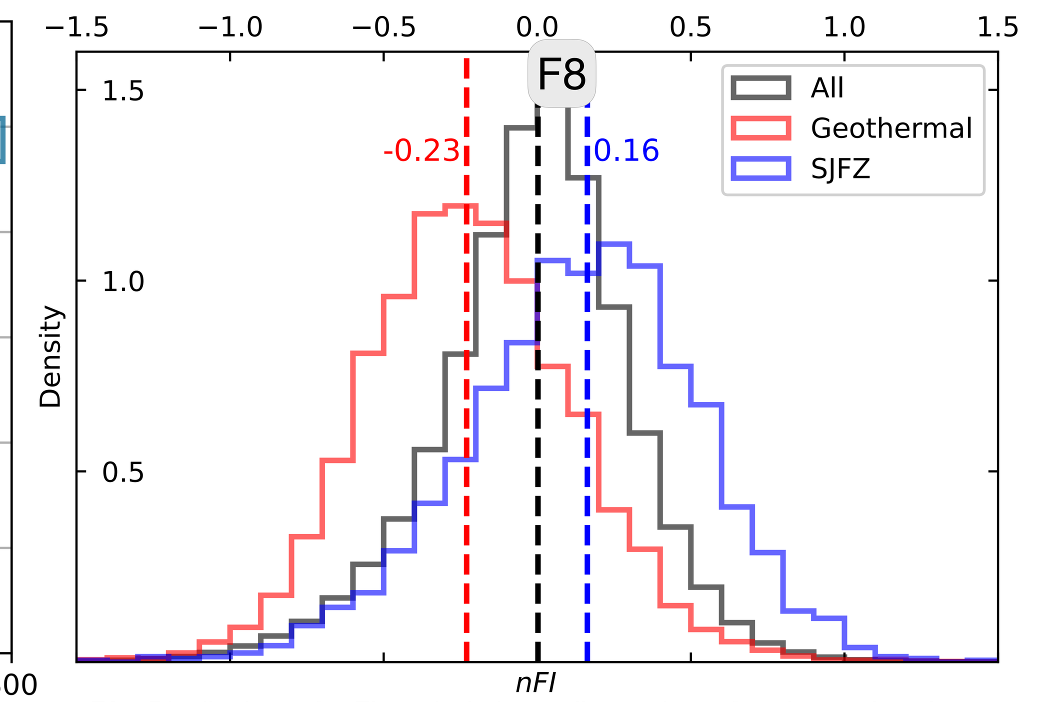

F8: Distribution of nFI and their median values for the entire dataset, earthquakes near geothermal wells, and earthquakes near the San Jacinto Fault Zone

nFI is low in geothermally-active regions with high heat flow

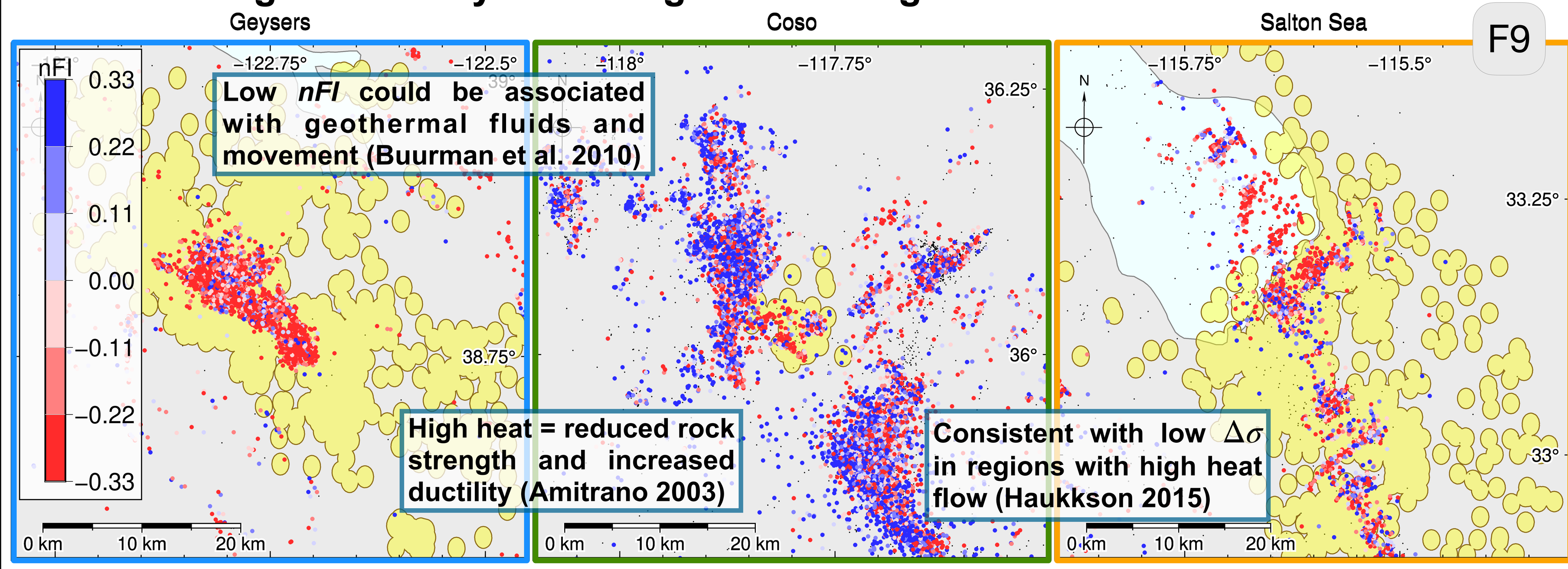

F9: Three geothermally-active regions: Geysers, Coso, and the Salton Sea, produce earthquakes with relatively less high-frequency energy. Yellow blobs show locations of geothermal wells.

nFI can correlate with local geology and volcanism

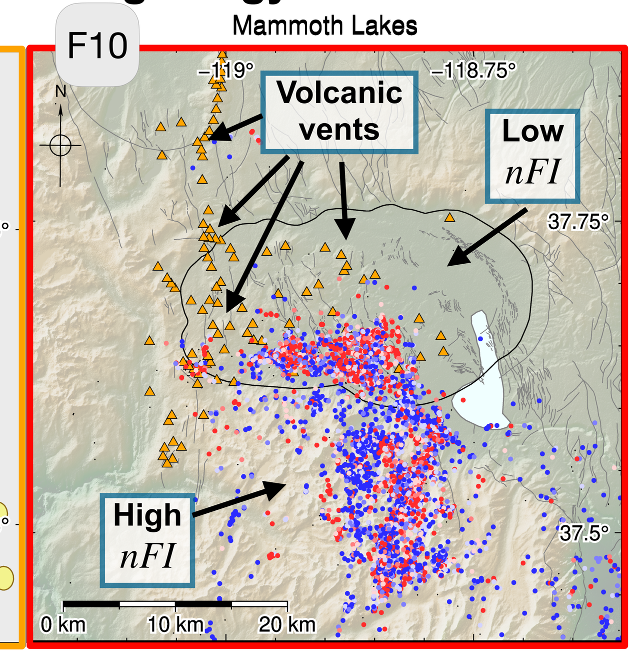

F10: Low-average nFI inside the Long Valley Caldera (-0.08), high-average outside (0.06). Black line indicates the Ring Fault along the edge of the caldera, grey lines indicate mapped faults, orange triangles are volcanic vents.

nFI exhibits smaller-scale spatial variation within aftershock sequences and high-seismicity regions

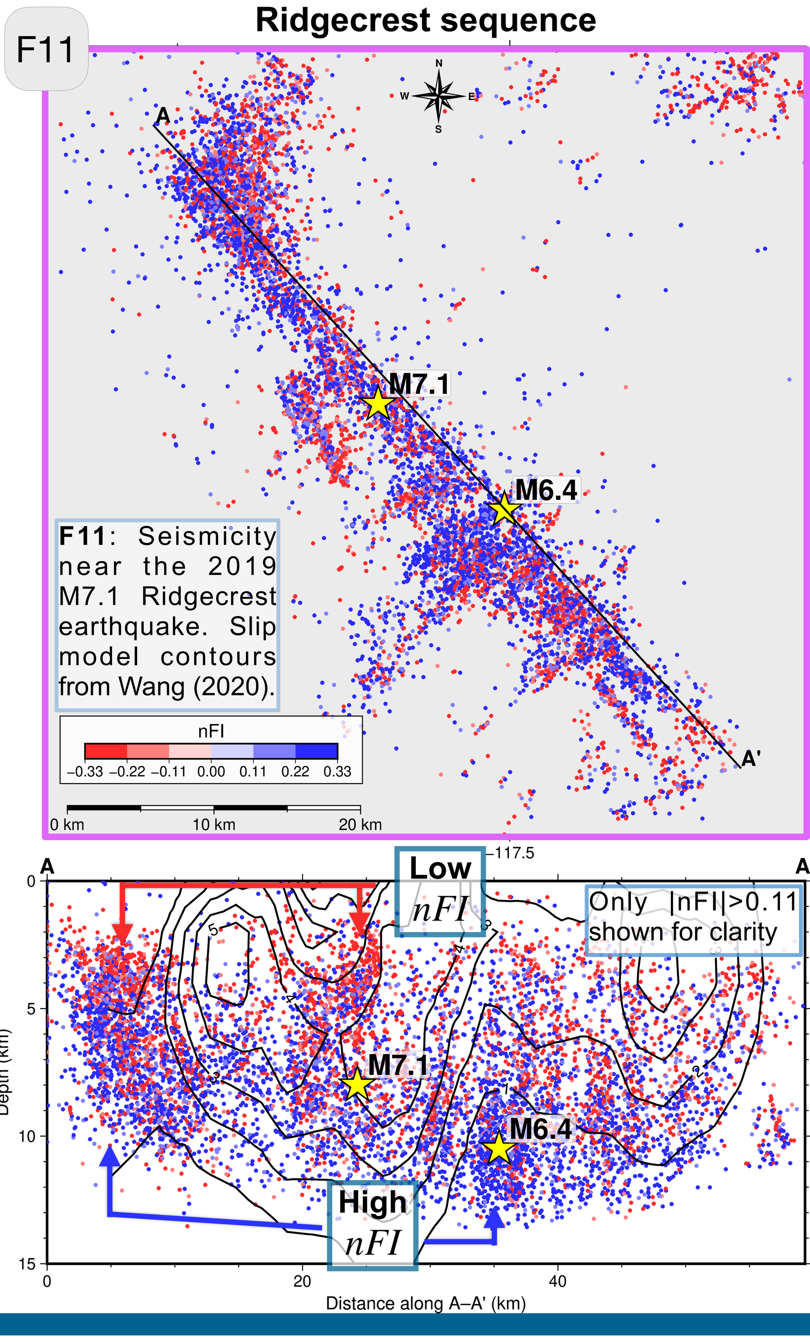

F11: Seismicity near the 2019 M7.1 Ridgecrest earthquake. Slip model contours from Wang (2020).

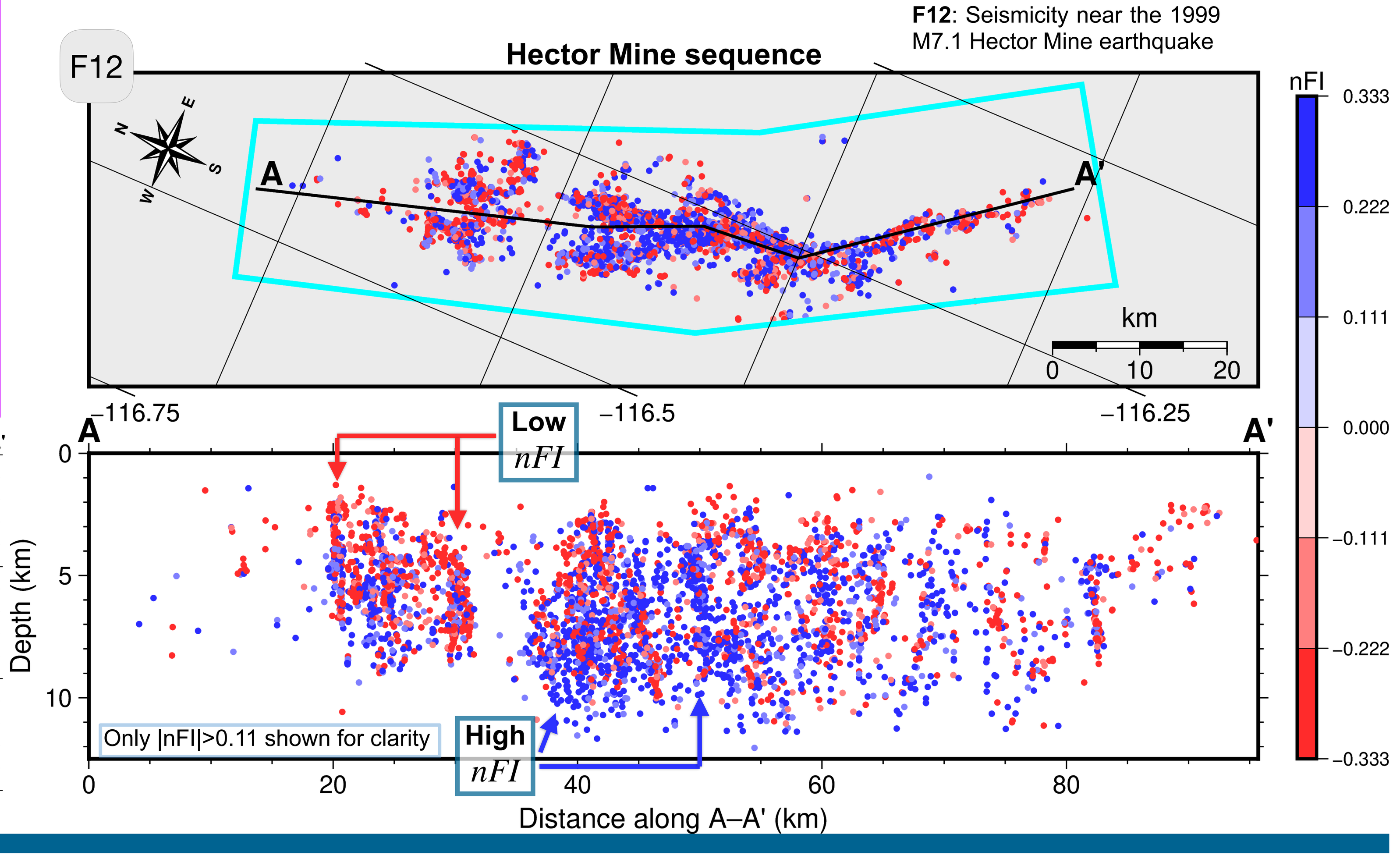

F12: Seismicity near the 1999 M7.1 Hector Mine earthquake

Takeaways

- We compute **P-wave** nFI, a metric that **quantifies an earthquake's relative high-frequency energy**, for 30 years of California seismicity.
- nFI has **coherent spatial variation** on a statewide-scale (**F4**) and local scale (**F9, F10, F11, F12**)
- nFI **increases with depth**, even when excluding shallow geothermally-active regions (**F7**)
- nFI is **low in geothermally-active regions** (**F7, F8, F9**), including areas with mapped volcanic vents (**F10**) possibly due to a combination of higher ductility and presence of fluids
- Faults with **more recent slip have lower** nFI (**F6**), suggesting less healing time, weaker fault strength, and lower stress drop.

Try it on your dataset! py-nfi on GitHub

Abstract

Acknowledgements

Funding for this research was provided by USGS and SCEC. Data was accessed from SCEDC and NCEDC services.

References

Abercrombie, R. E., Stress drops of repeating earthquakes on the San Andreas Fault at Parkfield. *Geophysical Research Letters*, 2014.
Abercrombie, R. E., Resolution and uncertainties in estimates of earthquake stress drop and energy release. *Philosophical Transactions of the Royal Society A: Mathematical, Physical and Engineering Sciences*, 2021.
Bailey, R.A., Geologic map of Long Valley caldera, Mono-Inyo Craters volcanic chain, and vicinity, Mono County, California. *U.S. Geological Survey Miscellaneous Investigations,* 1989.
Baltay, A., Abercrombie, R., Chu, S., Taira, T., The SCEC/USGS community stress drop validation study using the 2019 Ridgecrest earthquake sequence. *Seismica,* 2024.
Buurman, H., West, M. E., & Power, J. A., Seismic precursors to volcanic explosions during the 2006 eruption of Augustine Volcano. *USGS*, 2010.
Lucazeau, F., Analysis and Mapping of an Updated Terrestrial Heat Flow Data Set. *Geochemistry, Geophysics, Geosystems*, 2019.
Shearer, P. M., R. E. Abercrombie, and D. T. Trugman, Improved stress drop estimates for M 1.5 to 4 earthquakes in Southern California from 1996 to 2019, *J. Geophys. Res.*, 2022.
Vandevert, I., P.M. Shearer, and W. Fan, Using a High- to Low-Frequency Spectral Ratio to Distinguish Variations in Earthquake Source Properties, *BSSA (accepted)*, 2026.
Wang, K., D. S. Dreger, E. Tinti, R. Bürgmann, and T. Taira, Rupture process of the 2019 Ridgecrest, California Mw 6.4 foreshock and Mw 7.1 earthquake constrained by seismic and geodetic data, *Bull. Seismol. Soc. Am.,* 2020.